

# Optical and hall properties of Al-doped ZnO thin films fabricated by pulsed laser deposition with various substrate temperatures

Seong Jun Kang · Yang Hee Joung

Received: 31 October 2012 / Accepted: 28 November 2012 / Published online: 7 December 2012  
© Springer Science+Business Media New York 2012

**Abstract** The 3 wt% Al-doped zinc oxide (AZO) thin films were fabricated on quartz substrates at a fixed oxygen pressure of 200 mTorr with various substrate temperatures (room temp.  $\sim 500$  °C) by using pulsed laser deposition in order to investigate the microstructure, optical, and electrical properties of AZO thin films. All thin films were shown to be c-axis oriented, exhibiting only a (002) diffraction peak. The AZO thin film, fabricated at 200 mTorr and 400 °C, showed the highest (002) orientation and the full width at half maximum (FWHM) of the (002) diffraction peak was  $0.42^\circ$ . The c-axis lattice constant decreased with increasing substrate temperature. The electrical property indicated that the highest carrier concentration ( $1.27 \times 10^{21} \text{ cm}^{-3}$ ) and the lowest resistivity ( $6.72 \times 10^{-4} \Omega\text{cm}$ ) were obtained in the AZO thin film fabricated at 200 mTorr and 400 °C. The optical transmittance in the visible region was higher than 80 %. The Burstein-Moss effect, which shifts to a high photon energy, was observed.

## 1 Introduction

Transparent conductive oxide (TCO) has been accepted as transparent electrode in solar cell and flat panel display [1–3]. Today, indium tin oxide (ITO) thin film has been widely selected as suitable TCO due to its notable electrical and optical characteristics. However, ITO thin film has many disadvantage. Aluminum-doped zinc oxide (AZO) thin film can be considered a right replacement for ITO thin film because it is more stable, more abundant, less

expensive, non-toxic material compare to ITO thin film. Further AZO thin film is highly conductive and transparent in the visible region [4–6].

Research on the AZO thin film has been mainly for sputtering or sol-gel method. Annealing effect and thermal stability of thin film using sputtering method [5, 7] and structural property according the variation of Al doping density for the thin film using sol-gel method have been studied [8]. But AZO thin film using pulsed laser deposition (PLD) method has been seldom studied.

PLD is a promising method of fabrication of oxide thin film such as high-quality ZnO, because of the creation of ablated particles with high energy in the plume produced from the laser source. PLD has many advantages such as fabricating thin film under the oxygen partial pressure, having high deposition rate, and keeping consistent stoichiometric proportion of thin film composite [9, 10]. However it is not well studied to fabricate the AZO thin film using PLD method. Particularly, investigation on the electrical, optical and structural properties of the AZO thin film using PLD method is seldom reported in the literature.

In this study, we fabricate 3 wt% Al doped ZnO thin films on quartz substrates as a function of variation in oxygen pressure and substrate temperature by using PLD method. We systematically study the influence of substrate temperature on the structural, optical, and electrical properties of AZO thin film using PLD method. We think that our results promote further research on the fabrication of AZO thin film using PLD method.

## 2 Experimental procedure

AZO thin films were fabricated on quartz substrates by using PLD method. The chamber was evacuated to a base

S. J. Kang · Y. H. Joung (✉)  
Department of Electrical & Semiconductor Engineering,  
Chonnam National University, Yeosu 550-749, South Korea  
e-mail: jyanghee@chonnam.ac.kr

pressure of  $5 \times 10^{-6}$  Torr. The Al-doped ZnO target (97 wt% ZnO + 3 wt% Al<sub>2</sub>O<sub>3</sub>) was a ceramic target with a 1-inch diameter and 0.25-inch thickness. The KrF laser (Lambda Physics, Compex 205), with a wavelength of 248 nm, was focused onto the target. The laser energy density was 2.0 J/cm<sup>2</sup>. The target was rotated continuously to produce a uniform plume. The substrate was placed at 60 mm from the target. In this work, AZO thin films were fabricated at substrate temperatures, from 27 (Room Temperature) to 500 °C, with a fixed oxygen pressure of 200 mTorr.

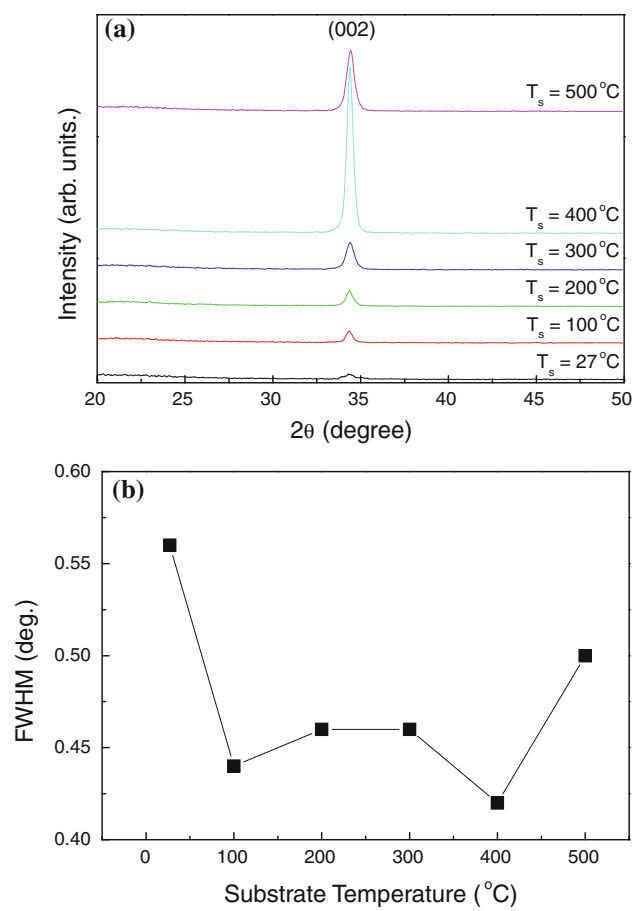
After deposition, the structural properties of the AZO thin films were investigated by X-ray Diffraction (XRD) measurements (Philips, PW 3020) with CuK $\alpha$  radiation ( $\lambda = 1.5406$  Å). AFM (VG, Microlab 310F) was used to characterize the surface morphology of the AZO thin films. The optical properties of the AZO thin films were characterized by a UV-vis spectrophotometer (Varian, Cary 500). The electrical properties were measured by van der Pauw Hall measurements (Accent, HL5500PC).

### 3 Results and discussion

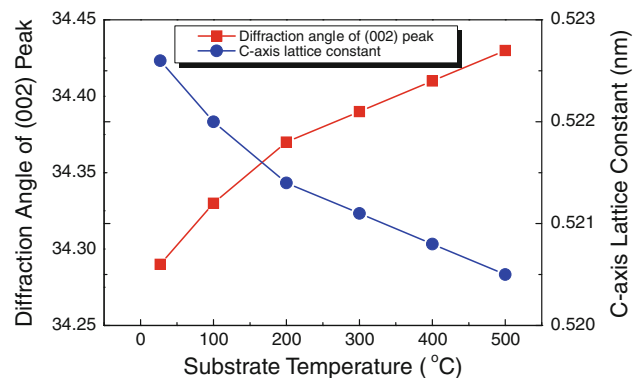
Figure 1a and b show the XRD spectra and the FWHM (Full-width at Half maximum) values of AZO thin films fabricated on quartz substrates by using PLD method at a fixed oxygen pressure of 200 mTorr with various substrate temperatures. All films showed only a (002) diffraction peak indicating that the c-axis of the grains was uniformly perpendicular to the substrate surface. The reason for (002) orientation has the lowest surface energy in AZO crystal. We found that the crystal quality of AZO thin films was strongly dependent on the substrate temperature. The AZO thin film fabricated at room temperature showed a relatively low (002) peak. However, with the substrate temperature up to 400 °C, the intensity of the (002) diffraction peak increased and the value of FWHM is decreased from 0.54 to 0.42°. At a higher temperature, the good quality of AZO thin film was the result of the enhancement of the mobility of adatoms caused by the supply of sufficient thermal energy. On the other hand, at a substrate temperature of 500 °C, the intensity of the (002) diffraction peak decreased. This indicated that the adatoms on the AZO thin film were decomposed and re-evaporated from the surface [11].

Figure 2 shows the diffraction angle of the (002) peak and the value of the c-axis lattice constant calculated from XRD patterns of AZO thin films (Fig. 1). Since the AZO thin film was a hexagonal structure, the lattice constant could be calculated by Bragg's law and Eq. (1)

$$\frac{1}{d_{hkl}^2} = \frac{4}{3} \left( \frac{h^2 + hk + k^2}{a^2} \right) + \frac{1}{c^2} \quad (1)$$



**Fig. 1** a XRD patterns and b FWHM values for AZO thin films fabricated at a fixed oxygen pressure of 200 mTorr with various substrate temperatures



**Fig. 2** The diffraction angle of (002) peak and c-axis lattice constant from XRD patterns for AZO thin films fabricated at a fixed oxygen pressure of 200 mTorr with various substrate temperatures

where,  $d$  was the distance of the (002) plane;  $h$ ,  $k$ ,  $l$  were the Miller's indices.

The position of the (002) diffraction peak shifted from 34.29 to 34.43° with increasing substrate temperature from 27 to 500 °C. It is observed that the (002) peak position

shifts towards the value (34.42°) of bulk ZnO with increasing substrate temperature up to 400 °C, but after 500 °C, the (002) peak position deviate from the value of bulk ZnO. The c-axis lattice constant, calculated from the XRD peak position for all AZO films, was in the range of between 0.5226 and 0.5205 nm, which was larger than the JCPDS value of 0.5207 nm for ZnO powder [12]. This phenomenon was because of the difference of ionic radius of Zn<sup>2+</sup> (0.074 nm) and Al<sup>3+</sup> (0.054 nm) and the thermal expansion coefficient mismatch between AZO thin film and the substrate [13]. On the other hand, the value of the c-axis lattice constant approached that of the bulk with increasing substrate temperature. This was probably due to the substitution Al<sup>3+</sup> ions, where the interstitial sites occupied, for Zn<sup>2+</sup> sites in the AZO crystal.

In order to investigate the effect of thermal conditions for AZO thin films, we calculated the stress of AZO thin films by using Eq. (2) [14]

$$\sigma = -453.6 \times \frac{c - c_0}{c_0} [\text{GPa}] \quad (c_0 = 0.5207 \text{ nm}) \quad (2)$$

where *c* and *c*<sub>0</sub> are the c-axis lattice constant calculated from the XRD peak position of AZO thin films and strain-free c-axis lattice constant, respectively. As the substrate temperature is increased, the value of stress for the AZO thin films was in the range from −1.66 to 0.17 GPa. The negative sign meant that the AZO thin films were in a state of compressive stress. But after 500 °C, the state of stress converted to the tensile stress. This result indicated that the stress in AZO thin films could strongly dependent on the thermal energy. In this study, the AZO thin film grown at 400 °C showed adjacent to the strain-free ZnO.

Through the above structural analysis, the good quality AZO thin film with minimum stress was fabricated at the substrate temperature of 400 °C.

Figure 3 shows AFM images (2 μm × 2 μm) for the AZO thin films fabricated at a fixed oxygen pressure of 200 mTorr with various substrate temperatures. As seen in Fig. 3, the surface morphology of AZO thin films showed a dense surface. At the substrate temperature of 400 °C, the largest grains were observed. The root mean square (RMS) roughness were 1.46, 3.60, 3.89, 3.98, 4.24 and 6.65 nm for AZO thin films with substrate temperature of 27, 100, 200, 300, 400 and 500 °C, respectively. As the substrate temperature increases, the RMS roughness also increased. We think that the coarse surface was due to the increase of grain size. On the other hand, at the substrate temperature of 500 °C, the AZO thin film exhibited the roughest surface, having a surface roughness of 6.65 nm. It is considered that this tendency is influenced by the volatilization of adatoms on the surface, because of the supply of the excessive thermal energy.

Figure 4 shows the results of the electrical properties for AZO thin films measured by a van der Pauw Hall

measurement at a fixed oxygen pressure of 200 mTorr with various substrate temperatures. Generally, we know that the n-type conductivity in non-stoichiometric ZnO is due to the presence of Zn interstitials (Zn<sub>i</sub><sup>+</sup>) and oxygen vacancies (V<sub>o</sub><sup>+</sup>). These defects in ZnO are easily ionized and electrons produced by ionized defects contribute to electrical conductivity. As a result, both Zn interstitials and oxygen vacancies play an important role in ZnO thin film's electrical conductivity and act as donors in the crystal. On the other hand, the doping of group-III (such as B, Al, In, Ga) resulted in higher electrical conductivity than un-doped ZnO thin film. These dopants replaced the Zn<sup>2+</sup> site or located in the interstitial sites in the crystal. This phenomenon caused the increase of the carrier concentration. The carrier concentration is increased from 5.87 × 10<sup>18</sup> to 1.27 × 10<sup>21</sup> cm<sup>-3</sup> and the resistivity is decreased from 0.45 to 6.72 × 10<sup>-4</sup> Ωcm with increasing substrate

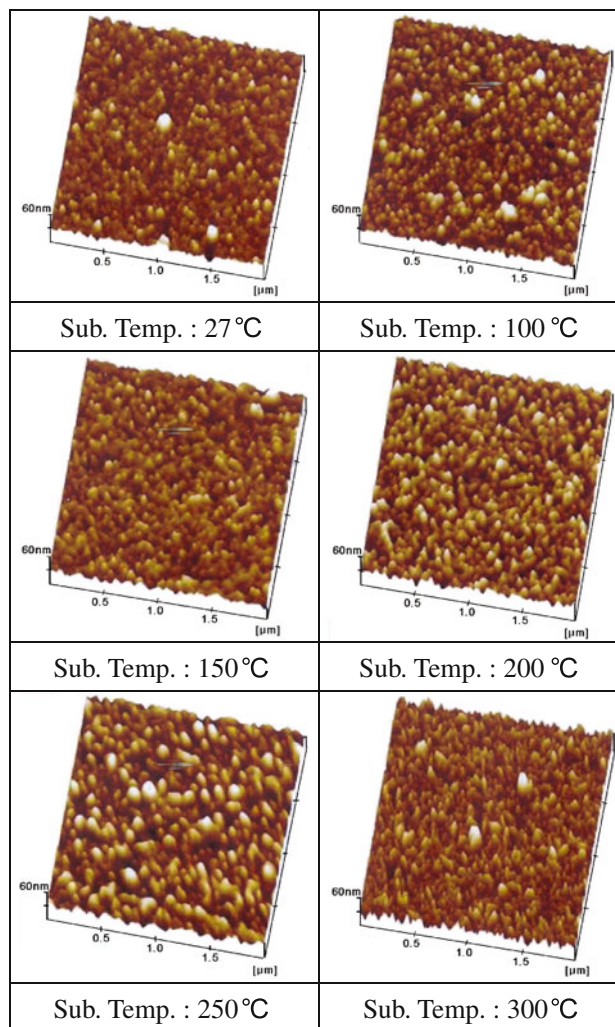
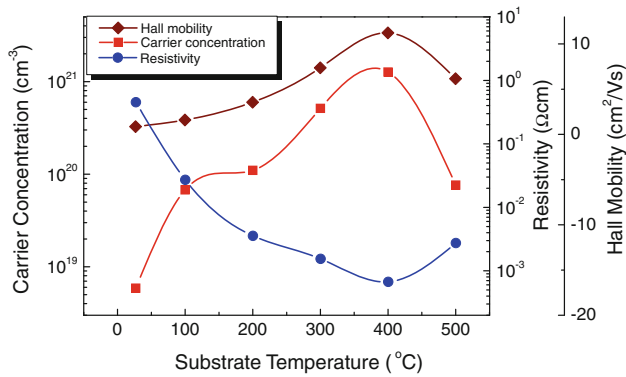


Fig. 3 The AFM images for AZO thin films fabricated at a fixed oxygen pressure of 200 mTorr with various substrate temperatures



**Fig. 4** The carrier concentration (filled square), Resistivity (filled circle) and Hall mobility (filled diamond) for AZO thin films fabricated at a fixed oxygen pressure of 200 mTorr with various substrate temperatures

temperature up to 400 °C. But at the substrate temperature of 500 °C, the decrease of carrier concentration ( $7.63 \times 10^{19} \text{ cm}^{-3}$ ) and the increase of resistivity ( $2.74 \times 10^{-3} \text{ } \Omega\text{cm}$ ) were observed. The carrier mobility also showed the same tendency as with the carrier concentration. At the substrate temperature of 400 °C, the highest carrier mobility of  $11.24 \text{ cm}^2/\text{Vs}$  was observed. The enhancement of carrier mobility may be explained to the improvement of crystallinity which decreased the number of scattering electrons in the grain boundary. However, at the substrate temperature of 500 °C, the carrier mobility decreased to  $6.17 \text{ cm}^2/\text{Vs}$ . The cause may be due to the increase of the ionized impurity scattering and grain boundary scattering [15].

In this study, the highest electrical conductivity of AZO thin films was obtained at the substrate temperature of 400 °C.

Figure 5 shows the optical transmittance spectra for AZO thin films fabricated at a fixed oxygen pressure of 200

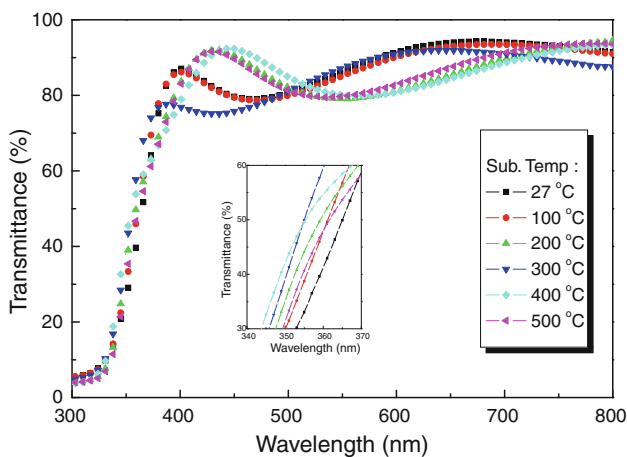


**Fig. 5** The transmittance spectra for AZO thin films fabricated at a fixed oxygen pressure of 200 mTorr with various substrate temperatures

mTorr with various substrate temperatures. All AZO thin films exhibited transparency of higher than 80 % in the visible region with a sharp absorption edge. The substrate temperature did not significantly have an effect on the transparency of the AZO thin films. We observed that the absorption edge of the AZO thin films shifted to a short wavelength with the substrate temperature up to 400 °C. The blue shift was related to the increase of carrier concentration indicating the broadening of the optical band gap.

Figure 6a shows the plots of  $(\alpha h\nu)^2$  versus  $h\nu$  for AZO thin films fabricated at a fixed oxygen pressure of 200 mTorr with various substrate temperatures. The absorption coefficient ( $\alpha$ ) can be calculated from the transmittance (T) and thickness (d) of the AZO thin films. The equation is followed by Eq. (3)

$$T = \exp(-\alpha d) \quad (3)$$

Since the AZO thin film had a direct band gap, the optical band gap for direct interband transition was given by Eq. (4) [16]

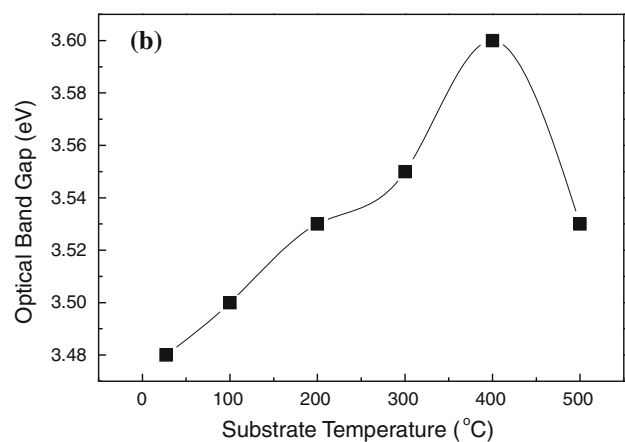
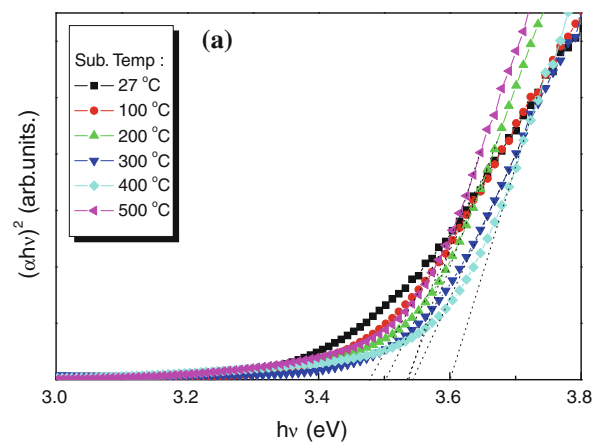


**Fig. 6 a** The spectra of  $(\alpha h\nu)^2$  versus  $h\nu$  for AZO thin films and **b** the optical band gap for AZO thin films fabricated at a fixed oxygen pressure of 200 mTorr with various substrate temperatures



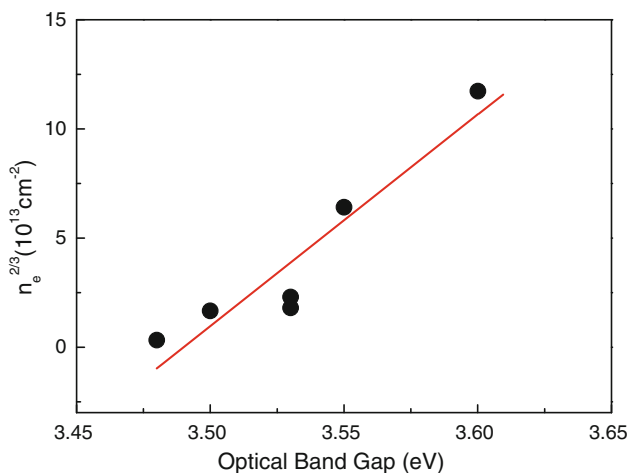


**Fig. 7** Dependence of optical band gap widening on the carrier concentration for AZO thin films

$$(\alpha h\nu)^2 = A(h\nu - E_g) \tag{4}$$

where A was the constant for a direct transition  $h\nu$  was the photon energy.

The optical band gap ( $E_g$ ) can be determined by extrapolation of the curve until the point where  $(\alpha h\nu)^2$  is zero. From Fig. 6b, the optical band gap is increased from 3.48 to 3.60 eV with increasing substrate temperature up to 400 °C. However, at the substrate temperature of 500 °C, the optical band gap decreased to 3.53 eV.

The widening of the optical energy band gap is expressed by Eq. (5) [17]

$$\Delta E_g = \frac{h^2}{8m^*} \left(\frac{3}{\pi}\right)^{2/3} n_e^{2/3} \tag{5}$$

where  $\Delta E_g$  denotes the shift in the doped semiconductor as compared to the undoped ZnO;  $m^*$ , the electron effective mass in the conduction band;  $h$ , the Planck’s constant; and  $n_e$ , the electron carrier concentration.

Using the Eq. (5), the dependence of optical band gap on carrier concentration is illustrated in Fig. 7. It reveals that the optical band gap of the AZO thin films broadens with increasing carrier concentration. This is the Burstein-Moss effect, and is due to the increase of Fermi level in the conduction band of the degenerate semiconductor [18, 19]. However, the optical band gap obtained for these AZO thin films does not accurately follow Eq. (5). This may be due to the merging of an impurity band into the conduction band [20].

#### 4 Conclusion

AZO thin films were fabricated on quartz substrates at a fixed oxygen pressure of 200 mTorr with various substrate

temperatures by using PLD method. High-quality ZnO film with good crystallinity was obtained from the film fabricated at 200 mTorr, 400 °C. We found that the angle of X-ray diffraction peak shifted to a high angle and the c-axis lattice constant decreased with increasing substrate temperature up to 400 °C. The largest carrier concentration ( $1.27 \times 10^{21} \text{ cm}^{-3}$ ) and lowest resistivity ( $6.72 \times 10^{-4} \Omega\text{cm}$ ) were obtained in ZnO films fabricated at 200 mTorr, 400 °C. We think that the decrease of resistivity may be due to the increase of Hall mobility and carrier concentration. The optical transmittance of the AZO thin films was higher than 80 % in the visible region. The Burstein-Moss effect was observed.

This study showed that the properties of AZO films fabricated by using PLD method were strongly affected by the substrate temperatures. The study on the oxygen pressure and post-annealing for AZO thin films will facilitate its application as a transparent conductive oxide in the next generation.

**Acknowledgments** This study was financially supported by Chonnam National University, 2011.

#### References

1. Y. Hamesa, Z. Alpaslan, A. Kosemen, S.E. San, Y. Yerli, Sol. Energy **84**, 426 (2010)
2. U. Ozgur, Y.I. Alivov, C. Liu, A. Teke, M.A. Reshchikov, S. Dogan, V. Avrutin, S.J. Cho, H. Morkoc, J. Appl. Phys. **98**, 041301 (2005)
3. W.J. Jeong, S.K. Kim, G.C. Park, Thin Solid Films **180**, 506 (2006)
4. B.Y. Oh, M.C. Jeong, T.H. Moon, W. Lee, J.M. Myoung, J.Y. Hwang, J. Appl. Phys. **99**, 124505 (2006)
5. X.R. Deng, H. Deng, M. Wei, J.J. Chen, J. Mater. Sci. Mater. Electron. **23**, 413 (2012)
6. I.H. Kim, D.Y. Ku, J.H. Ko, D. Kim, K.S. Lee, J.H. Jeong, T.S. Lee, B. Cheong, Y.J. Baik, W.M. Kim, J. Electroceram. **17**, 241 (2006)
7. J. Huang, R. Tan, Y. Zhang, J. Li, Y. Yang, X. Zhang, W. Song, J. Mater. Sci. Mater. Electron. **23**, 356 (2012)
8. R. Chandramohan, V. Dhanasekaran, S. Ezhilvizhian, T.A. Vijayan, J. Thirumalai, A.J. Peter, T. Mahalingam, J. Mater. Sci. Mater. Electron. **23**, 390 (2012)
9. J.L. Zhao, X.M. Li, J.M. Bian, W.D. Yu, X.D. Gao, J. Cryst. Growth **276**, 507 (2005)
10. S.J. Kang, Y.H. Joung, H.H. Shin, Y.S. Yoon, J. Mater. Sci. Mater. Electron. **19**, 1073 (2008)
11. M. Liu, X.Q. Wei, Z.G. Zhang, G. Sun, C.S. Chen, C.S. Xue, H.Z. Zhuang, B.Y. Man, Appl. Surf. Sci. **252**, 4321 (2006)
12. JCPDS Card No. 79-2205
13. H. Kim, J.S. Horwitz, S.B. Qadri, D.B. Chrisey, Thin Solid Films **420–421**, 107 (2002)
14. M.K. Puchert, P.Y. Timbrell, R.N. Lamb, J. Vac. Sci. Technol. A **14**, 2220 (1996)
15. G. Fang, D. Li, B.L. Yao, Vacuum **68**, 363 (2003)

16. N. Kenny, C.R. Kannewurf, D.H. Whitmore, *J. Phys. Chem. Solids* **27**, 1237 (1996)
17. R.E. Dietz, J.J. Hopfield, D.G. Thomas, *J. Appl. Phys.* **32**, 2282–2286 (1961)
18. J.H. Park, H.H. Pak, C.R. Cho, *J. Korean Phys. Soc.* **49**, S584 (2006)
19. B.E. Sernelius, K.F. Berggren, Z.C. Jin, I. Hamberg, C.G. Granqvist, *Phys. Rev. B* **37**, 10244 (1988)
20. Z.C. Jin, I. Hamberg, C.G. Granqvist, *J. Appl. Phys.* **17**, 279 (1998)